

# Theoretical Prediction of Topological Insulators in Thallium-based III-V-VI<sub>2</sub> Ternary Chalcogenides

Binghai Yan<sup>1</sup>, Chao-Xing Liu<sup>2</sup>, Hai-Jun Zhang<sup>3,4</sup>, Chi-Yung Yam<sup>1</sup>,  
Xiao-Liang Qi<sup>4,5</sup>, Thomas Frauenheim<sup>1</sup> and Shou-Cheng Zhang<sup>4</sup>

<sup>1</sup>*Bremen Center for Computational Materials Science,*

*Universität Bremen, Am Fallturm 1, 28359 Bremen, Germany*

<sup>2</sup>*Physikalisches Institut (EP3) and Institute for Theoretical Physics and Astrophysics,*

*University of Würzburg, 97074 Würzburg, Germany*

<sup>3</sup>*Beijing National Laboratory for Condensed Matter Physics,*

*and Institute of Physics, Chinese Academy of Sciences, Beijing 100190, China*

<sup>4</sup>*Department of Physics, McCullough Building, Stanford University, Stanford, CA 94305-4045*

<sup>5</sup>*Microsoft Research, Station Q, Elings Hall, University of California, Santa Barbara, CA 93106, USA*

(Dated: February 5, 2021)

We predict a new class of three dimensional topological insulators in thallium-based III-V-VI<sub>2</sub> ternary chalcogenides, including TlBiQ<sub>2</sub> and TlSbQ<sub>2</sub> (Q = Te, Se and S). These topological insulators have robust and simple surface states consisting of a single Dirac cone at the  $\Gamma$  point. The mechanism for topological insulating behavior is elucidated using both first principle calculations and effective field theory models. Remarkably, one topological insulator in this class, TlBiTe<sub>2</sub> is also a superconductor when doped with *p*-type carriers. We discuss the possibility that this material could be a topological superconductor. Another material TlSbS<sub>2</sub> is on the border between topological insulator and trivial insulator phases, in which a topological phase transition can be driven by pressure.

PACS numbers:

Topological insulators have attracted great attention in condensed matter physics<sup>1</sup>. Since the first theoretical prediction<sup>2</sup> and the subsequent experimental observation<sup>3</sup> in HgTe quantum wells, several other topological insulators in three dimensional (3D) bulk materials have been theoretically predicted and experimentally observed<sup>4-8</sup>. In particular, tetradymite semiconductors Bi<sub>2</sub>Te<sub>3</sub>, Bi<sub>2</sub>Se<sub>3</sub>, and Sb<sub>2</sub>Te<sub>3</sub> are predicted to be topological insulators with a large bulk band gap whose surface state consists of a single Dirac cone<sup>6</sup>. The mechanism for the topological insulating behavior in these 3D materials is the band inversion at the  $\Gamma$  point caused by large spin-orbit coupling, similar to the mechanism first discovered in HgTe quantum wells<sup>2</sup>. The tetradymite semiconductors have a layered structure consisting of stacking quintuple layers, making surface preparation particularly simple.

In this work we predict a new class of 3D topological insulators in the thallium-based III-V-VI<sub>2</sub> ternary chalcogenides. These inversion symmetric topological insulators have a bulk energy gap and topologically protected surface states consisting of a single Dirac cone. Unlike the tetradymite semiconductors, these materials are intrinsically 3D, and do not have a weakly coupled layer structure. Nonetheless, effective field theory model describing the band electrons close to the Fermi energy takes the same form as the model proposed earlier for the tetradymite semiconductors<sup>6</sup>, and the mechanism for topological insulating behavior can be understood in a similar way.

The discovery of topological insulators also inspired the intense search for topological superconductors<sup>9-13</sup>. Time reversal invariant topological superconductors have a full

pairing gap in the bulk and topologically protected surface states consisting of Majorana fermions, see Fig 1 of Ref.<sup>9</sup>. Whereas Dirac fermions have both particle and hole types, Majorana fermions are their own antiparticles.<sup>14</sup> In the simplest version, the surface state of a 3D topological superconductor consists of a single Majorana cone, thus containing half the degree of freedom of the Dirac surface states of a simple 3D topological insulator. This fractionalization of the degree of freedom introduces quantum non-locality and is central to the program of topological quantum computing based on Majorana fermions<sup>15</sup>. Superfluid He<sup>3</sup>B phase has been proposed as an candidate for the 3D topological superfluid state, however, no example of a topological superconductor state has been found so far.

The most striking property of this new class of topological insulators is the superconductivity observed in *p* doped TlBiTe<sub>2</sub><sup>16</sup>. In this paper, we propose that the *p* doped TlBiTe<sub>2</sub> could inherit the topological properties from its parent topological insulator, and outline pairing scenarios under which the topological superconductor state could be realized.

Thallium-based III-V-VI<sub>2</sub> ternary chalcogenides have rhombohedral crystal structure with the space group  $D_{3d}^5$  (R $\bar{3}m$ ), which is similar to tetradymite semiconductors. We take TlBiTe<sub>2</sub> as an example. The crystal structure of TlBiTe<sub>2</sub> can be viewed as the distorted NaCl structure with four atoms in the primitive unitcell, which is shown in Fig 1 (a). These atoms are placed in layers normal to the three-fold axis with the sequence -Tl-Te-Bi-Te<sup>17</sup>. For Bi<sub>2</sub>Se<sub>3</sub>, five atomic layers form a quintuple layer and the coupling between two quintuple layers is very weak, of the van der Waals type<sup>6</sup>. However here the outmost

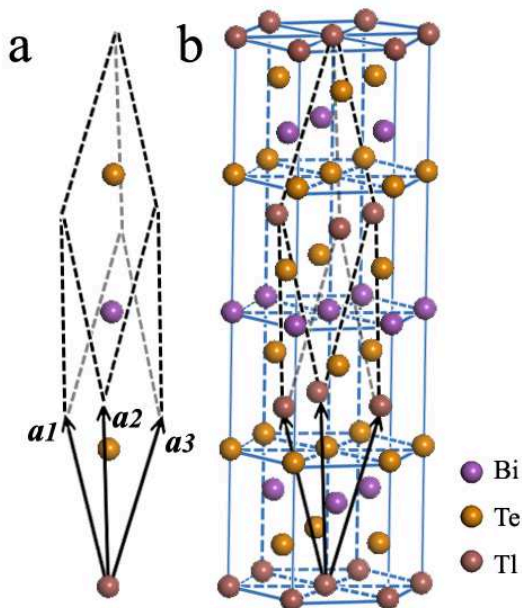


FIG. 1: Crystal structure. (a) Crystal structure of  $\text{TlBiTe}_2$  with three primitive lattice vectors denoted as  $\mathbf{a}_1, \mathbf{a}_2, \mathbf{a}_3$ , including four atoms. (b) The equivalent hexagonal lattice of  $\text{TlBiTe}_2$  with atomic layers stacked in the sequence -Tl-Te-Bi-Te-.

electron shells for Tl, Bi and Te are all p-orbitals ( $6p^1$  for Tl,  $6p^3$  for Bi and  $5p^4$  for Te) and each Tl (Bi) layer is sandwiched by two Te layers, therefore there is strong coupling between every two atomic layers for  $\text{TlBiTe}_2$  and the crystal structure is essentially 3D. Figure 1(b) shows the 3D layered structure with the rhombohedral unit cell of  $\text{TlBiTe}_2$ . Similar to  $\text{Bi}_2\text{Se}_3$ , there is inversion symmetry for this type of materials and both Tl and Bi sites act as the inversion center under an inversion operation.

To investigate the electronic band structure and topological property of these materials, we performed *ab initio* calculations within the density functional theory using the Perdew- Burke-Ernzerhof type generalized gradient approximation<sup>18</sup> and the projected augmented wave method<sup>19</sup> implemented in the *Vienna ab initio simulation package*<sup>20</sup>. The plane wave basis is used with energy cutoff of 300 eV. Spin-orbit coupling (SOC) is included except in ionic optimization. We optimized of lattice parameters and ionic positions first, and then used the relaxed structure to calculate electronic properties. The optimized lattice parameters agree with reported experimental<sup>17,21,22</sup> and theoretical<sup>23</sup> results. Our calculated band structures for these six materials are also consistent with previous calculations<sup>23</sup>. The electronic band structures of  $\text{TlBiSe}_2$  and  $\text{TlBiTe}_2$  without (dashed line) and with SOC (solid line) are shown in Fig. 2 (a) and (b), respectively. There is a large energy shift for the

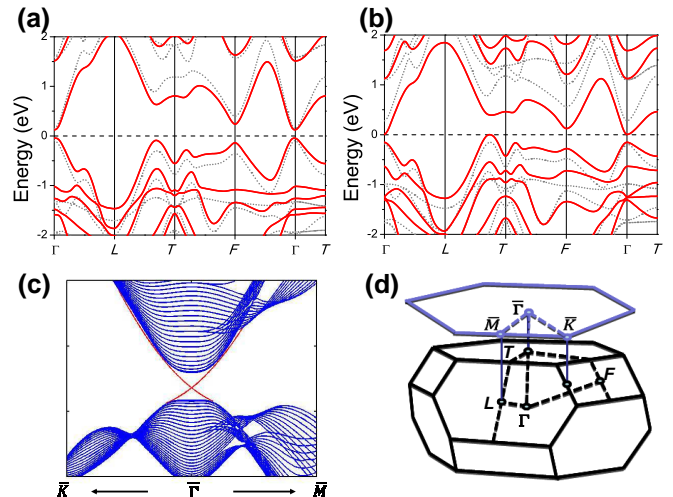


FIG. 2: Band structure, surface state and Brillouin zone. Band structure for (a)  $\text{TlBiSe}_2$  and (b)  $\text{TlBiTe}_2$  without (gray dotted lines) and with (red solid lines) SOC. The dashed line indicates the Fermi level. (c) The surface states (red line) shows a single Dirac cone for  $\text{TlBiSe}_2$ . The black line shows the band edge for conduction band and valence band. The dispersion of surface states are calculated from the effective Hamiltonian (4). (d) Brillouin zone for this class of materials. The four inequivalent time-reversal-invariant points are  $\Gamma(0;0;0)$ ,  $L(\pi;0;0)$ ,  $F(\pi;\pi;0)$  and  $T(\pi;\pi;\pi)$ . We further project the 3D bulk Brillouin zone into the plane of the atomic layer to obtain the surface Brillouin zone.

conduction and valence band and the band gap shrinks considerably when the SOC is turned on, indicating that the SOC plays an important role for this type of materials. The conduction band minimum (CBM) lies at  $\Gamma$  point for both  $\text{TlBiSe}_2$  and  $\text{TlBiTe}_2$ , while the valence band maximum (VBM) is at  $\Gamma$  point for  $\text{TlBiSe}_2$  and along the L-T line for  $\text{TlBiTe}_2$ . Therefore  $\text{TlBiSe}_2$  is a direct gap semiconductor while  $\text{TlBiTe}_2$  is an indirect narrow gap semiconductor, consistent with previous experiments and calculations<sup>23-25</sup>. In order to investigate the topological property of the system, we analyze the charge density of the VBM and CBM at the  $\Gamma$  point. Before SOC is included, the VBM is composed mainly by the Te- $p$  orbital and CBM mainly by the Bi- $p$  and Te- $sp$  orbitals. After SOC is turned on, VBM and CBM exchange their charge density characteristics, indicating that a band inversion may occur, just as in the case of  $\text{HgTe}$  quantum wells and  $\text{Bi}_2\text{Se}_3$  type of materials. To further determine the topological nature of the system, we follow the parity criteria proposed by Fu and Kane<sup>4</sup>, and calculate the product of the parity eigenvalues of the Bloch wavefunction for the occupied bands at all time-reversal-invariant momenta  $\Gamma, L, F, T$  in the Brillouin zone, both with and without SOC. For  $\text{TlSbS}_2$ , the product of the parity eigenvalues remains the same when the SOC is included, while for all the other materials

	Parity eigenvalues	Gap at $\Gamma$	Bulk gap (eV)
TlBiTe <sub>2</sub>	+ - + + - - - + + - ; +	(-)	0.16 <0.01*
TlBiSe <sub>2</sub>	+ - + + - - - + + - ; +	(-)	0.17 0.17
TlBiS <sub>2</sub>	+ - + + - - - + + - ; +	(-)	0.07 0.07
TlSbTe <sub>2</sub>	+ - + + - - - + + - ; +	(-)	0.05 0.05
TlSbSe <sub>2</sub>	+ - + + - - - + + - ; +	(-)	0.19 0.14*
TlSbS <sub>2</sub>	+ - + + - - - + + - ; -	(+)	0.09 0.04*

\* Indirect gap.

FIG. 3: Table: the parity of the band at the  $\Gamma$  point and the band gap for the six materials. Here, we show the parity eigenvalues of ten occupied bands and the lowest unoccupied band. The product of the parity eigenvalues for the ten occupied bands is given in brackets on the right of each row. We list the band gap both at the  $\Gamma$  point and in the whole Brillouin zone (bulk gap) in unit of eV.

in this class, the parity eigenvalue of one occupied band (VBM) at  $\Gamma$  point changes after turning on SOC, and the parity eigenvalues for all the occupied bands at  $L, F, T$  do not change. The parity eigenvalues of the total 10 valence bands and the first conduction band at  $\Gamma$  point, as well as the band gaps are listed in Table 1. From the parity analysis we find that TlSbS<sub>2</sub> is a trivial insulator and all the other materials in this class are strong topological insulators. Although TlSbS<sub>2</sub> is a trivial insulator, it sensitively depends on the lattice constant. We find that about 2% compressive strain along the  $c$ -axis in the hexagonal lattice will induce a band inversion between the conduction and valence bands and the corresponding pressure is less than 2 GPa, which is reachable under ambient condition. Therefore this material opens the exciting possibility to systematically study the topological quantum phase transition between 3D topological insulators and normal insulators by tuning pressure.

As discussed above, the band inversion only occurs at the  $\Gamma$  point, therefore it is helpful to investigate the effective Hamiltonian near the  $\Gamma$  point, which can be constructed from the symmetry property of the system. To derive the effective Hamiltonian, we need to identify at  $\Gamma$  point the representations of the crystal symmetry group for both the conduction and the valence bands. Here we denote the conduction band as  $P1^+$  band and the valence band as  $P2^-$  band, where  $\pm$  denotes the parity of the corresponding bands. With the spin degeneracy, four bands ( $(|P1^+, \uparrow\rangle, |P2^-, \uparrow\rangle, |P1^+, \downarrow\rangle, |P2^-, \downarrow\rangle)$ ) need to be taken into account for the effective Hamiltonian. The crystal structure of TlBiTe<sub>2</sub> belongs to  $D_{3d}^5$ , which is same to that of Bi<sub>2</sub>Se<sub>3</sub>. Thus the wave functions

at  $\Gamma$  point can also be classified according to the symmetry group of  $D_{3d}^5$ , similarly as we have done for Bi<sub>2</sub>Se<sub>3</sub><sup>26</sup>. According to the irreducible representation of the space group  $D_{3d}^5$ , we find that the conduction band belongs to the  $\Gamma_6^+$  representation while the valence band belongs to the  $\Gamma_6^-$  representation. Consequently, the four band effective Hamiltonian of Bi<sub>2</sub>Se<sub>3</sub> is still valid here, which in the basis of ( $|P1^+, \uparrow\rangle, |P2^-, \uparrow\rangle, |P1^+, \downarrow\rangle, |P2^-, \downarrow\rangle$ ) reads<sup>6,26</sup>

$$H(\mathbf{k}) = H_0(\mathbf{k}) + H_3(\mathbf{k}) \quad (1)$$

$$H_0(\mathbf{k}) = \epsilon_0(\mathbf{k})I_{4 \times 4} +$$

$$\begin{pmatrix} \mathcal{M}(\mathbf{k}) & -iA_1k_z & 0 & iA_2k_- \\ iA_1k_z & -\mathcal{M}(\mathbf{k}) & iA_2k_- & 0 \\ 0 & -iA_2k_+ & \mathcal{M}(\mathbf{k}) & -iA_1k_z \\ -iA_2k_+ & 0 & iA_1k_z & -\mathcal{M}(\mathbf{k}) \end{pmatrix} \quad (2)$$

$$H_3(\mathbf{k}) = \frac{R_1}{2} \begin{pmatrix} 0 & K_+ & 0 & 0 \\ K_+ & 0 & 0 & 0 \\ 0 & 0 & 0 & -K_+ \\ 0 & 0 & -K_+ & 0 \end{pmatrix} + \frac{R_2}{2} \begin{pmatrix} 0 & -K_- & 0 & 0 \\ K_- & 0 & 0 & 0 \\ 0 & 0 & 0 & -K_- \\ 0 & 0 & K_- & 0 \end{pmatrix} \quad (3)$$

with  $k_{\pm} = k_x \pm ik_y$ ,  $\epsilon_0(\mathbf{k}) = C + D_1k_z^2 + D_2k_{\perp}^2$ ,  $\mathcal{M}(\mathbf{k}) = M - B_1k_z^2 - B_2k_{\perp}^2$  and  $K_{\pm} = k_{\pm}^3 \pm k_{\mp}^3$ . Here  $H_0(\mathbf{k})$  is the effective Hamiltonian expanded up to the  $k$  quadratic term, which preserve the in-plane rotation symmetry.  $H_3(\mathbf{k})$  is the  $k$ -cubic term which breaks the in-plane rotation symmetry down to the three fold rotation symmetry. Combining the  $\mathbf{k} \cdot \mathbf{p}$  perturbation theory with the *ab initio* calculation<sup>26</sup>, we can numerically calculate the parameters of our model, giving  $C = -0.045\text{eV}$ ,  $M = 0.087\text{eV}$ ,  $A_1 = 1.330\text{eV} \cdot \text{\AA}$ ,  $A_2 = 2.821\text{eV} \cdot \text{\AA}$ ,  $D_1 = 6.338\text{eV} \cdot \text{\AA}^2$ ,  $D_2 = 11.140\text{eV} \cdot \text{\AA}^2$ ,  $B_1 = 0.342\text{eV} \cdot \text{\AA}^2$ ,  $B_2 = 18.225\text{eV} \cdot \text{\AA}^2$ ,  $R_1 = 14.367\text{eV} \cdot \text{\AA}^3$  and  $R_2 = 43.331\text{eV} \cdot \text{\AA}^3$  for TlBiTe<sub>2</sub>. The parameters  $M > 0$ ,  $B_1 > 0$  and  $B_2 > 0$  indicate that the system stays in the inverted regime and is topologically non-trivial. The topologically non-trivial surface states can be directly calculated from the above four band model by imposing proper boundary condition<sup>6,27,28</sup>. Taking a semi-infinite sample where the Hamiltonian (1) applies only for  $z > 0$ , it can be shown that two localized states  $|\psi_{\uparrow}\rangle$  and  $|\psi_{\downarrow}\rangle$  appear at  $k_x = k_y = 0$  which are time-reversal partner of each other. We can further project the effective Hamiltonian (1) onto the subspace spanned by these two localized states, which yields<sup>26</sup>

$$H_{sur} = \tilde{C} + \tilde{D}_2k_{\parallel}^2 + \tilde{A}_2(k_x\sigma_y - k_y\sigma_x) + \frac{\tilde{R}_1}{2}(k_+^3 + k_-^3)\sigma_z \quad (4)$$

up to  $k^3$ . Here the parameters  $\tilde{C}$ ,  $\tilde{D}_2$ ,  $\tilde{A}_2$ , and  $\tilde{R}_1$  depend on the detail of the boundary condition<sup>26</sup> and material parameters<sup>28</sup>. For simplicity, we just take bulk values for these parameters, the energy dispersion for the topologically nontrivial surface states are plotted in the Fig 2(c), which shows a single Dirac cone at  $\Gamma$  point, similar to the case of Bi<sub>2</sub>Se<sub>3</sub>. For Bi<sub>2</sub>Se<sub>3</sub>, due to the weak

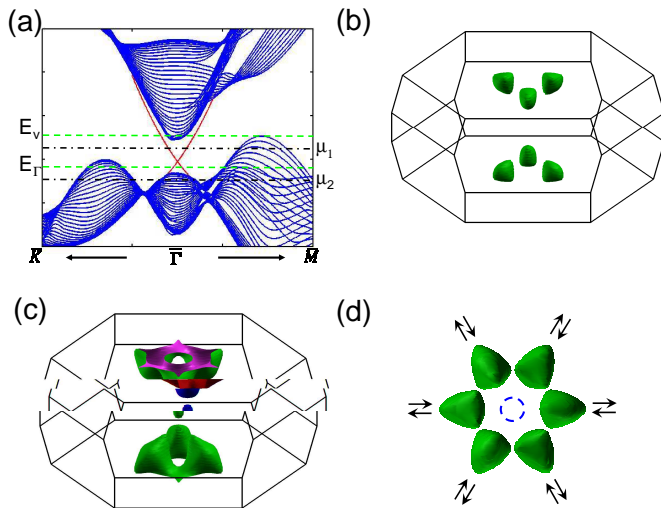


FIG. 4: Superconductivity in  $TlBiTe_2$ . a. Bulk and surface states of  $TlBiTe_2$ .  $E_v$  and  $E_\Gamma$  are the valence band top in the whole Brillouin zone and at  $\Gamma$  point, respectively.  $\mu_1$  and  $\mu_2$  labels two typical positions of chemical potential. b and c. Fermi surface shape corresponding to  $\mu_1$  and  $\mu_2$  respectively. d. Schematic picture of the He<sup>3</sup>-B type triplet pairing with spin direction correlated with momentum.

coupling between two quintuple layers, the clean surface can be easily obtained in experiment. For  $TlBiSe_2$ , as we have pointed out above, every two atomic layers are strongly coupled, and consequently, trivial surface states with dangling bonds may exist on a cleaved surface. However these trivial surface states will not change the topological property of the system.

Among the predicted materials,  $TlBiTe_2$  is observed to be a superconductor with  $p$ -type carrier.<sup>16</sup>  $TlBiTe_2$  has an indirect gap, with 6 hole pockets around the  $T$  point upon hole doping, as shown in Fig. 4 b and c. Compared with the other five materials in this family, which either have an indirect gap comparable with the  $\Gamma$  point gap or have a direct gap, it is natural to expect that the 6 hole pockets around the  $T$  point are responsible for the superconductivity in  $TlBiTe_2$ . Depending on the

position of the chemical potential, there are two distinct superconducting phases possible, as shown in Fig. 4 a. First, when the chemical potential lies below the top of the valence band  $E_v$ , but still above the top of the valence band at the  $\Gamma$  point  $E_\Gamma$ , topological surface states around the  $\Gamma$  point coexist with the 6 bulk hole fermi pockets. In the superconducting state, the surface states can also become superconducting due to proximity effect with the bulk states. As proposed by Fu and Kane<sup>29</sup>, each vortex of such a superconductor has a Majorana zero mode, making this system a new candidate for topological quantum computation<sup>15</sup>. Compared to the Cu doped  $Bi_2Se_3$  superconductor discovered recently<sup>30</sup>, the coexistence between topological surface states and bulk superconductivity in  $TlBiTe_2$  is much better defined, because of the well-separation of the surface and bulk states in momentum space. Second, when the chemical potential lies below  $E_\Gamma$ , the topological surface states are not well-defined any more, and a bulk hole pocket appears around  $\Gamma$  point. When the hole pocket around  $\Gamma$  point is small compared to the pre-existing 6 hole pockets, the pairing symmetry at the  $\Gamma$  point pocket is determined by that of the 6 pockets through proximity effect in momentum space. If the 6 hole pockets have the same sign of pairing amplitude, the resulting superconducting state is topologically trivial. However, since Tl d-orbital characters are generally present for the wave functions of the hole pockets, Coulomb correlation effects maybe important, and inter-pocket repulsive scattering generally prefer opposite signs of pairing amplitudes on different pockets. This mechanism implies a negative “Josephson coupling” between different pockets. However, due to the three-fold symmetry of the fermi surface, such a coupling is frustrated, so that the pairing order parameter in the ground state may become complex. A natural choice of such a complex orbital pairing symmetry without breaking the time reversal symmetry is a triplet pairing symmetry similar to the BW state in He3 B-phase, as illustrated in Fig. 4 d. When the hole pocket around Gamma point appears, the proximity effect from such a pairing symmetry leads to a topological superconductor with a nodeless bulk gap, and a gapless surface state consisting of a single branch of Majorana fermions.

<sup>1</sup> Qi, X.-L. & Zhang, S.-C. The quantum spin hall effect and topological insulators. *Physics Today* **63**, 33 (2010).

<sup>2</sup> B. A. Bernevig, T. L. Hughes & S.C. Zhang. Quantum spin hall effect and topological phase transition in hgte quantum wells. *Science* **314**, 1757 (2006).

<sup>3</sup> König, M. *et al.* Quantum spin hall insulator state in hgte quantum wells. *Science* **318**, 766–770 (2007).

<sup>4</sup> Fu, L. & Kane, C. L. Topological insulators with inversion symmetry. *Phys. Rev. B* **76**, 045302 (2007).

<sup>5</sup> Hsieh, D. *et al.* A topological dirac insulator in a quantum spin hall phase. *Nature* **452**, 970–974 (2008).

<sup>6</sup> Zhang, H. *et al.* Topological insulators in  $Bi_2Se_3$ ,  $Bi_2Te_3$  and  $Sb_2Te_3$  with a single Dirac cone on the surface. *Nature Physics* **5**, 438–442 (2009).

<sup>7</sup> Xia, Y. *et al.* Observation of a large-gap topological-insulator class with a single dirac cone on the surface. *Nat Phys* **5**, 398–402 (2009).

<sup>8</sup> Chen, Y. L. *et al.* Experimental realization of a Three-Dimensional topological insulator,  $Bi_2Te_3$ . *Science* **325**, 178–181 (2009).

<sup>9</sup> Qi, X.-L., Hughes, T. L., Raghu, S. & Zhang, S.-C. Time-reversal-invariant topological superconductors and super-

- fluids in two and three dimensions. *Phys. Rev. Lett.* **102**, 187001 (2009).
- <sup>10</sup> Qi, X.-L., Hughes, T. L. & Zhang, S.-C. Fermi surface topological invariants for time reversal invariant superconductors. *arxiv:cond-mat/0908.3550* (2009).
- <sup>11</sup> Schnyder, A. P., Ryu, S., Furusaki, A. & Ludwig, A. W. W. Classification of topological insulators and superconductors in three spatial dimensions. *Phys. Rev. B* **78**, 195125 (2008).
- <sup>12</sup> Kitaev, A. Periodic table for topological insulators and superconductors. *Proceedings of the L.D.Landau Memorial Conference "Advances in Theoretical Physics". Arxiv preprint 0901.2686* (2009).
- <sup>13</sup> Roy, R. Topological superfluids with time reversal symmetry. *Arxiv preprint 0803.2868* (2008).
- <sup>14</sup> Wilczek, F. Majorana returns. *Nat Phys* **5**, 614–618 (2009).
- <sup>15</sup> Nayak, C., Simon, S. H., Stern, A., Freedman, M. & Sarma, S. D. Non-abelian anyons and topological quantum computation. *Rev. Mod. Phys.* **80**, 1083 (2008).
- <sup>16</sup> Hein, R. & Swiggard, E. Superconductivity in TlBiTe<sub>2</sub>: a low carrier density (III-V)VL<sub>2</sub> compound. *Phys. Rev. Lett.* **24**, 53–55 (1970).
- <sup>17</sup> Hockings, E. F. & White, J. G. The crystal structures of TlSbTe<sub>2</sub> and TlBiTe<sub>2</sub>. *Acta Crystallographica* **14**, 328 (1961).
- <sup>18</sup> Perdew, J. P., Burke, K. & Ernzerhof, M. Generalized gradient approximation made simple. *Phys. Rev. Lett.* **77**, 3865 (1996).
- <sup>19</sup> Kresse, G. & Joubert, D. From ultrasoft pseudopotentials to the projector augmented-wave method. *Phys. Rev. B* **59**, 1758–1775 (1999).
- <sup>20</sup> Kresse, G. & Furthmüller, J. Efficient iterative schemes for ab initio total-energy calculations using a plane-wave basis set. *Phys. Rev. B* **54**, 11169–11186 (1996).
- <sup>21</sup> Madelung, O. *Semiconductors: Data Handbook* (Springer-Verlag, 2004), 3rd edn.
- <sup>22</sup> Ozer, M., Paraskevopoulos, K. M., Anagnostopoulos, A. N., Kokou, S. & Polychroniadis, E. K. Large single-crystal growth and characterization of the narrow-gap semiconductor. *Semiconductor Science and Technology* **11**, 1405–1410 (1996).
- <sup>23</sup> Hoang, K. & Mahanti, S. D. Atomic and electronic structures of thallium-based *iii-v-vi2* ternary chalcogenides: Ab initio calculations. *Phys. Rev. B* **77**, 205107 (2008).
- <sup>24</sup> Paraskevopoulos, K. M. Energy gap dependence on temperature in TlBiTe<sub>2</sub> crystals. *J. Mater. Sci. Lett.* **6**, 1422–1424 (1987).
- <sup>25</sup> Jensen, J. D., Burke, J. R., Ernst, D. W. & Allgaier, R. S. Structural and electrical properties of tlbite<sub>2</sub> and tlte. *Phys. Rev. B* **6**, 319–327 (1972).
- <sup>26</sup> Liu, C., Zhang, H., Qi, X. & Zhang, S. unpublished.
- <sup>27</sup> Koenig, M. *et al.* The quantum spin hall effect: Theory and experiment. *J. Phys. Soc. Japan* **77**, 031007 (2008).
- <sup>28</sup> Shan, W., Lu, H. & Shen, S. Effective continuous model for surface states and thin films of three dimensional topological insulators. *arxiv:cond-mat/1001.0526* (2010).
- <sup>29</sup> Fu, L. & Kane, C. L. Superconducting proximity effect and majorana fermions at the surface of a topological insulator. *Phys. Rev. Lett.* **100**, 096407 (2008).
- <sup>30</sup> Wray, L. *et al.* Observation of unconventional band topology in a superconducting doped topological insulator, CuxBi<sub>2</sub>Se<sub>3</sub>: topological superconductor or non-Abelian superconductor? *Arxiv: cond-mat/0912.3341* (2009).